Integrating INS Sensors With GPS Measurements for Continuous Estimation of Vehicle Sideslip, Roll, and Tire Cornering Stiffness

David M. Bevly, Jihan Ryu, and J. Christian Gerdes

***Abstract*—This paper details a unique method for estimating key vehicle states—body sideslip angle, tire sideslip angle, and vehicle attitude—using Global Positioning System (GPS) measurements in conjunction with other sensors. A method is presented for integrating Inertial Navigation System sensors with GPS measurements to provide higher update rate estimates of the vehicle states. The influence of road side-slope and vehicle roll on estimating vehicle sideslip is investigated. A method using one GPS antenna that estimates accelerometer errors occurring from vehicle roll and sensor drift is first developed. A second method is then presented utilizing a two-antenna GPS system to provide direct measurements of vehicle roll and heading, resulting in improved sideslip estimation. Additionally, it is shown that the tire sideslip estimates can be used to estimate the tire cornering stiffnesses. The experimental results for the GPS-based sideslip angle measurement and cornering stiffness estimates compare favorably to theoretical predictions, suggesting that this technique has merit for future implementation in vehicle safety systems.**

***Index Terms*—Global Positioning System (GPS)/Inertial Navigation System (INS) vehicle state estimation, GPS sideslip measurements, roll estimation, sideslip estimation.**

I. Introduction

MANY VEHICLE control systems, such as antilock braking (ABS), stability control, and vehicle lateral control schemes, require vehicle sideslip as critical component of the control logic [1]–[3]. Unfortunately, this value is not typically available without the presence of expensive speed-over-ground sensors. To compensate for the lack of a direct measurement, the common practice on production systems is to integrate inertial sensors in order to obtain slip angle estimates [2]–[5]. However, this integration is prone to drift and can be corrupted by road bank angle and vehicle roll [6], forcing many production algorithms to intervene based on changes in slip angle rate instead of slip angle. Although in some cases, nonlinear observers can estimate the slip angle from yaw rate measurements [7], the slip angle cannot be observed using yaw rate and steer angle as the vehicle approaches neutral steer characteristics. Other methods for estimating vehicle sideslip angle from dynamic and kinematic models [8] or by switching between model estimation and accelerometer integration based on judgments of vehicle spinout or bank angle [9] require accurate knowledge of uncertain tire parameters. This fundamental lack of a sideslip angle measurement, coupled with uncertainty in the parameters needed for model-based estimation, places severe constraints on stability control algorithms and other potential vehicle dynamics control [3].

The Global Positioning System (GPS) has provided the ability to determine a body's position, velocity, and attitude anywhere on the surface of the globe and has proven effective when implemented on vehicles for navigation [10] and lanekeeping [11]. With the absence of selective availability (SA), a GPS receiver can provide very accurate three-dimensional velocity measurements without the need for any differential corrections (known as differential GPS or DGPS). The standard deviation of the GPS velocity noise, which depends on the satellite geometry, varies from approximately 3–5 cm/s in the horizontal axis and 6–10 cm/s in the vertical axis [27]. These velocity accuracies provide a measure of the direction of travel of the vehicle to within 0.1° at speeds above 10 m/s [27], where vehicle stability control and sideslip estimation is critical. A GPS receiver with multiple antennas can provide attitude measurements with an accuracy of 0.4° (with a baseline length of 1 m) [12]. Additionally, the integration of Inertial Navigation System (INS) with GPS has been given much attention due to the complementary nature of the short-term errors in GPS measurements and long-term errors in INS measurements. While low-cost inertial sensors can be noisy and biased, integration of these sensors with GPS velocity measurements can provide high-update nonbiased estimates of vehicle states, including sideslip. Research has been directed toward updating position estimates with inertial equipment between low-rate (1–5 Hz) GPS measurements [13], [14], utilizing inertial units during short GPS outages [15]–[17], augmenting GPS with INS for land navigation/location systems [18], estimating roll parameters [19], and even automating highway systems [20]. Recent GPS/INS work has also been extended to include magnetometers [21], wheel speed sensors [22], and vehicle constraints [23].

Two system setups are presented and compared in this paper. First, a one-antenna GPS system is proposed. The GPS receiver's computed velocity measurements are used to estimate both the true vehicle velocity vector heading and the yaw rate sensor's bias, whereas the integrated yaw rate sensor provides

Manuscript received July 26, 2005; revised March 30, 2006, May 18, 2006, and June 24, 2006. The Associate Editor for this paper was R. Goudy.

D. M. Bevly is with the Department of Mechanical Engineering, Auburn University, Auburn, AL 36849-5341 USA (e-mail: dmbevly@eng.auburn.edu).

J. Ryu is with General Motors R&D and Planning, Warren, MI 48090-9055 USA (e-mail: jihan.ryu@gm.com).

J. C. Gerdes is with the Department of Mechanical Engineering, Stanford University, Stanford, CA 94305-4021 USA (e-mail: gerdes@stanford.edu).

Color versions of Figs. 3–18 are available at http://www.ieeexplore.ieee.org.

Digital Object Identifier 10.1109/TITS.2006.883110

the vehicle frame heading. The yaw rate sensor's bias can be estimated only when the vehicle is going straight. This system could be based around existing receivers for navigation or other in-car services. Alternatively, a two-antenna GPS system is proposed to provide vehicle heading and roll. Since vehicle roll measurements are available with the two-antenna system, the effect of road side-slope in sideslip estimation is shown. The availability of a road side-slope measurement is shown to improve the sideslip estimates from that of the one-antenna system. Road grade can be estimated by examining the ratio of vertical velocity to horizontal velocity from a one-antenna GPS receiver [24]. However, because the longitudinal motion of vehicle dominates over the lateral motion, a two-antenna GPS receiver is required to estimate the road side-slope properly. A two-antenna GPS receiver whose antennas are placed laterally can provide the ability to determine the vehicle roll and heading. Such systems have been used successfully to provide aircraft heading information [14], [25] as well as calibrate aircraft sideslip angle sensors [26]. Research has already shown that the velocity measurements can be used to provide measurements of wheel slip and vehicle sideslip on highway vehicles [27]. Although GPS is susceptible to loss of signal due to satellite blockages, this paper focuses on the capabilities that can be realized when GPS is available.

Because the vehicle parameters are not used in the estimation of vehicle sideslip, a separate algorithm can be used to identify the parameters of the bicycle model. In this paper, the estimated sideslip from a kinematic Kalman filter is used to identify the front and rear cornering stiffness of the tires when the vehicle is turning, thus producing a sideslip angle. Most vehicle electronic stability control systems require accurate knowledge of the cornering stiffness to function properly [2], [3]. Therefore, the tire cornering stiffness data can be used to improve control and estimation schemes, such as stability control, steer-by-wire controller design, and lateral control on an automated highway, or diagnostic systems that monitor tire condition and friction detection algorithms.

The methodology for GPS/INS combination and cornering stiffness estimation is demonstrated on a Mercedes E-class sedan. The test vehicle is equipped with a Novatel OEM4 GPS antenna/receiver pair that provides 10-Hz velocity measurements and a two-antenna Novatel Beeline GPS receiver that provides attitude (i.e., yaw and roll) measurements at 5 Hz. The vehicle is equipped with a three-axis inertial measurement unit (IMU) sampled at 200 Hz as well as a front steer angle and wheel speed sensor sampled at 50 Hz. The IMU consists of three automotive grade accelerometers and rate gyroscopes mounted orthogonal to each other, which were developed by Robert Bosch Corporation for stability control systems. The sensor accuracies (1σ) are 5 cm/s for the GPS velocity, 0.006 m/s^2 for the lateral accelerometer, 0.08°/s for the yaw rate sensor, and 0.4° for the two-antenna GPS attitude measurements.

II. System Model

Fig. 1 shows a schematic of half of a vehicle. (This is known as the bicycle model.) The heading angle ψ and the course angle ν are referenced from the horizontal X-axis, whereas the sideslip angle β is referenced from the vehicle's longitudinal x-axis [28]. The bicycle model has been shown to be effective for use in vehicle estimation control systems [2], [3], [29]. The linear differential equations describing the lateral and yaw dynamics for the bicycle model are given by

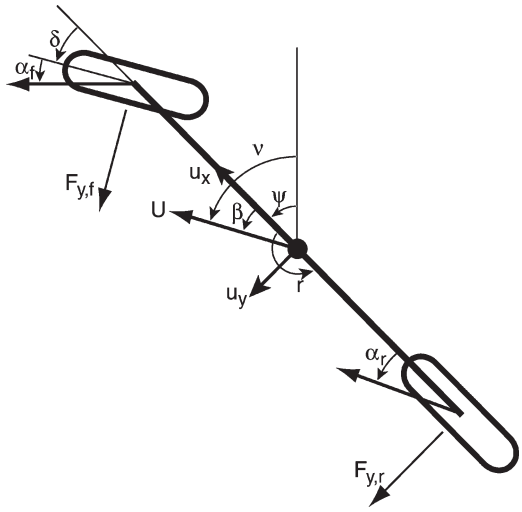

Fig. 1. Schematic of the bicycle model.

$$\begin{bmatrix}\dot{u}_y\\ \dot{r}\end{bmatrix}=\begin{bmatrix}\frac{-C_{\alpha f}-C_{\alpha r}}{mu_x} & -u_x+\left(\frac{C_{\alpha r}b-C_{\alpha f}a}{mu_X}\right)\\ \frac{C_{\alpha r}b-C_{\alpha f}a}{I_z u_x} & \frac{-C_{\alpha f}a^2-C_{\alpha r}b^2}{I_z u_X}\end{bmatrix}\begin{bmatrix}u_y\\ r\end{bmatrix}+\begin{bmatrix}\frac{C_{\alpha f}}{m}\\ \frac{C_{\alpha f}a}{I_z}\end{bmatrix}\delta \tag{1}$$

where

a	distance from the front axle to the center of gravity (CG);
b	distance from the rear axle to the CG;
$C_{\alpha f}, C_{\alpha r}$	front and rear tire cornering stiffnesses (per axle);
m	vehicle mass;
I_Z	yaw moment of inertia of the vehicle;
u_x	longitudinal velocity;
u_y	lateral velocity;
r	yaw rate;
δ	steer angle.

The vehicle used for experimental validation in this paper had a mass and yaw moment of inertia of 1640 kg and 3500 kg $\cdot$ m^2, respectively. The wheel base length is 2.8 m with 54% of the vehicle weight on the front axle ($a = 1.3$ and $b = 1.5$). The front and rear tire cornering stiffness are 100 000 and 160 000 N/° per axle, respectively. The bicycle model shown in (1) was used with the vehicle parameters listed above to simulate the vehicle for comparison with the experimentally measured states in the subsequent sections. While it is important to note that the yaw model above is derived with a constant velocity assumption, a more complex model that includes velocity variation can be developed. However, typical speeds for maneuvers in this paper were 7–10 m/s, varying by ∼1–2 m/s on any given run. Therefore, the model described above was considered adequate for modeling the dynamics under these circumstances.

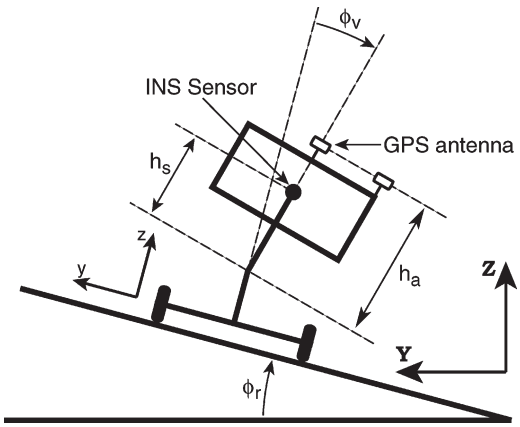

Fig. 2. Roll center model with road side-slope.

Fig. 2 shows the roll coordinates for the vehicle using a simple roll center model with road side-slope. The relationship between the attitude changes of vehicle in the Earth-fixed coordinates and the angular velocities in the vehicle-frame-fixed coordinates is expressed by

$$\begin{aligned}\dot{\phi} &= \omega_x + (\sin\phi \cdot \tan\theta) \cdot \omega_y + (\cos\phi \cdot \tan\theta) \cdot \omega_z \\ \dot{\theta} &= \cos\phi \cdot \omega_y - \sin\phi \cdot \omega_z \\ \dot{\psi} &= \frac{\sin\phi}{\cos\theta} \cdot \omega_y + \frac{\cos\phi}{\cos\theta} \cdot \omega_z \end{aligned} \tag{2}$$

where

ϕ, θ, ψ	vehicle roll, pitch, and yaw angle in the Earth-fixed coordinates;
$\omega_x, \omega_y, \omega_z$	angular velocities in the vehicle-frame-fixed coordinates.

Since the lateral dynamics of the vehicle are of most concern, the relationship in (2) can be simplified by considering only yaw and roll motions, which are defined as follows:

$$\begin{aligned}\dot{\phi} &= \omega_x \\ \dot{\psi} &= \cos\phi \cdot \omega_z \end{aligned} \tag{3}$$

assuming $\theta \approx 0$ and $\omega_y \approx 0$.

Using (3), the kinematic relationship between the sensor (lateral accelerometer and the roll and yaw gyroscope) measurements and the vehicle states can be written as

$$\begin{aligned} a_{y,m} &= \dot{u}_{y,\text{frame}} + \dot{\psi} \cdot u_{x,\text{frame}} + g \cdot \sin(\phi_r + \phi_v) \\ &\quad - (c \cdot \ddot{\psi} + h \cdot \ddot{\phi}_v) \cdot \cos\phi_v + a_{y,\text{bias}} + w_1 \\ p_m &= \dot{\phi}_r + \dot{\phi}_v + p_{\text{bias}} + w_2 \\ r_m &= \dot{\psi}/\cos(\phi_r + \phi_v) + r_{\text{bias}} + w_3 \end{aligned} \tag{4}$$

where

$u_{y,\text{frame}}$	lateral velocity of the vehicle frame;
$u_{x,\text{frame}}$	longitudinal velocity of the vehicle frame;
ϕ_r	roll angle of the vehicle frame due to road side-slope;
ϕ_v	roll angle of the vehicle body due to suspension;
ψ	yaw angle of the vehicle frame;
$a_{y,m}$, $a_{y,\text{bias}}$	lateral accelerometer measurement and bias;
p_m, p_{bias}	roll rate gyro measurement and bias;
r_m, r_{bias}	yaw rate gyro measurement and bias;
c	longitudinal distance from accelerometer location to CG;
h	vertical distance from accelerometer location to roll center;
w	serially uncorrelated sensor noise.

Note that the third term in the lateral accelerometer measurement equation is from gravity, which could be the main source of accelerometer errors. The fourth term is from the vehicle yaw and roll effect. This term is usually not zero because it is not practically possible in many cases to place sensors at either the vehicle CG or the vehicle roll center. Because the angular acceleration measurements $\ddot{\phi}$ and $\ddot{\psi}$ are not available, this term should be either 1) evaluated by numerical differentiation of the rate gyro or 2) ignored, assuming small effects. Either method is shown to be feasible by the analysis of actual test data. Results from experiments show that there is no noticeable difference between the two methods because the bias term $a_{y,\text{bias}}$ can take account of possible errors in each case.

III. State and Parameter Estimation

As discussed previously, vehicle control systems require estimates of vehicle sideslip, tire slip angles, and tire cornering stiffness. The body sideslip angle (β in Fig. 1) is the simply the difference between the vehicle yaw and vehicle course (or direction of travel) measured at the CG of the vehicle, i.e.,

$$\beta = \nu - \psi. \tag{5}$$

The relationship between the lateral velocity u_y and the vehicle sideslip is simply

$$u_y = U\sin(\beta). \tag{6}$$

The measured slip angle is the slip angle of the vehicle at the antenna. In contrast, it is usually desired to know the slip angle either at the vehicle CG or at the tires. In order to move the slip angle estimation from the GPS antenna to any point P on the vehicle, the velocity at antenna A must be transposed to that point with the addition of any velocity arising from vehicle angular velocity, i.e.,

$$U_P = U_A + \vec{\omega} \times \vec{r}_{A/P} \tag{7}$$

where $\vec{\omega}$ normally includes roll, pitch, and yaw rates of the vehicle. The slip angle at point P on the vehicle can then be calculated from the velocity components in each axis of the vehicle at that point, i.e.,

$$\beta_P = \tan^{-1}\left(\frac{u_y^P}{u_x^P}\right) \tag{8}$$

where u_x and u_y are the velocity components in the body-fixed coordinates.

The tire slip angle (α_f and α_r in Fig. 1) is the difference between the tire's longitudinal axis and its direction of travel. The direction of travel of each tire can be calculated by translating the vehicle velocity at the GPS antenna to the tire using either the simplified bicycle model or a full four-wheel representation. The direction of the rear tire axes is equal to the vehicle heading, whereas the direction of the front tires is calculated by adding in the steering angle. Ignoring camber effects, the slip angles of the front and rear tires can be found by moving the sideslip angle to the tire and incorporating the measurement of the steer angle as

$$\begin{aligned} \alpha_f &= \beta_f^{\text{tire}} - \delta \\ \alpha_r &= \beta_r^{\text{tire}}. \end{aligned} \tag{9}$$

With these tire sideslip angle measurements, the lateral accelerations from the accelerometer and the yaw rate measurements (minus the sensor biases from the Kalman filter estimation algorithm) can be used to provide an estimate of the front and rear tire cornering stiffness. Estimates of the tire cornering stiffness can be obtained in various ways, including analyzing the forces of the bicycle model (shown in Fig. 1) using Newton's equations. We now have

$$\begin{aligned} \sum F_y &= m\ddot{y} = F_{yf}\cos(\delta) + F_{yr} \\ \sum M_z &= I_z\ddot{\psi} = aF_{yf}\cos(\delta) - bF_{yr}. \end{aligned} \tag{10}$$

These equations can be solved simultaneously for the lateral front and rear tire forces. The lateral tire forces are then simply a function of the cornering stiffness as shown in the following equation:

$$\begin{aligned} F_{yf} &= 2C_{\alpha f}^{\text{tire}}\alpha_f = C_{\alpha f}^{\text{axle}}\alpha_f \\ F_{yr} &= 2C_{\alpha r}^{\text{tire}}\alpha_r = C_{\alpha r}^{\text{axle}}\alpha_r. \end{aligned} \tag{11}$$

The factor 2 in (11) is due to the fact the bicycle model lumps the left and right tires together. Alternatively, the two equations in the bicycle model given in (1) can be used to solve for the estimates of the front and rear cornering stiffness.

IV. Estimating Sideslip With INS Only

Current vehicle safety systems utilize inertial sensors to estimate vehicle sideslip. This section demonstrates some of the limitations of using inertial sensors to estimate sideslip. Fig. 3 shows the steer angle input and vehicle velocity for an experimental test consisting of two laps (8°–90° turns) around the top of a parking garage.

The vehicle sideslip is estimated by integrating a lateral accelerometer to obtain the lateral velocity. Note that vehicle sideslip is not observable from acceleration measurements alone, but this is the predominant method used to obtain sideslip in vehicle control systems [2], [3]. Additionally, because the accelerometer will measure lateral accelerations along with a gravity component due to vehicle roll and side-slope of the test surface [as shown in (4)], integration of the lateral accelerometer alone can lead to large errors in the sideslip estimation.

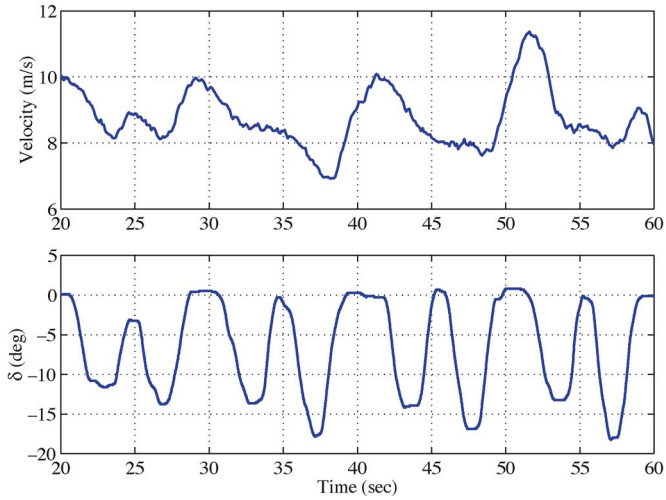

Fig. 3. Velocity and steer angle during experimental cornering maneuvers.

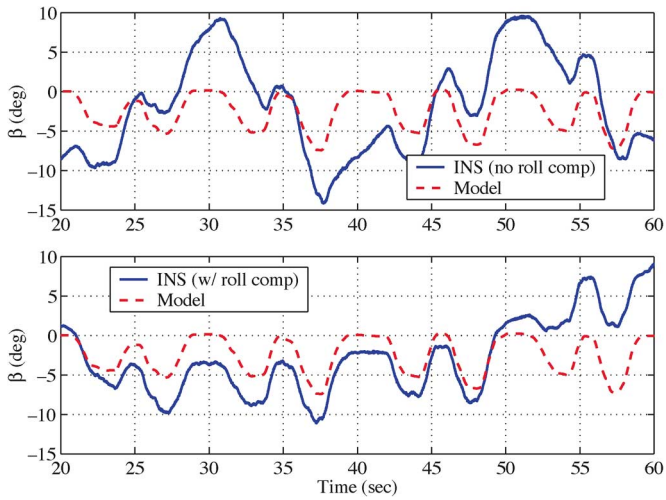

Fig. 4. Sideslip estimates using an accelerometer.

To demonstrate, a roll gyro was integrated to provide an estimate of vehicle roll. Fig. 4 shows the estimated sideslip angle from integration of the accelerometer with and without roll compensation. The roll estimate can then be used to compensate for the error component attributable to roll. Without this compensation, roughness of the sideslip estimation based on integrated accelerometers can be clearly seen. However, even with the compensation, the sideslip angle drifts and exhibits poor estimation of the vehicle sideslip angle produced by the bicycle model (and its assumption of a flat road surface).

V. GPS Velocity-Based Sideslip Determination

The main thrust of this paper is to show how GPS velocity measurements can be used to estimate vehicle sideslip. The GPS velocity measurements provide the vehicle course or direction of travel of the vehicle that must be compared to the vehicle heading or yaw to estimate the vehicle sideslip. The vehicle yaw

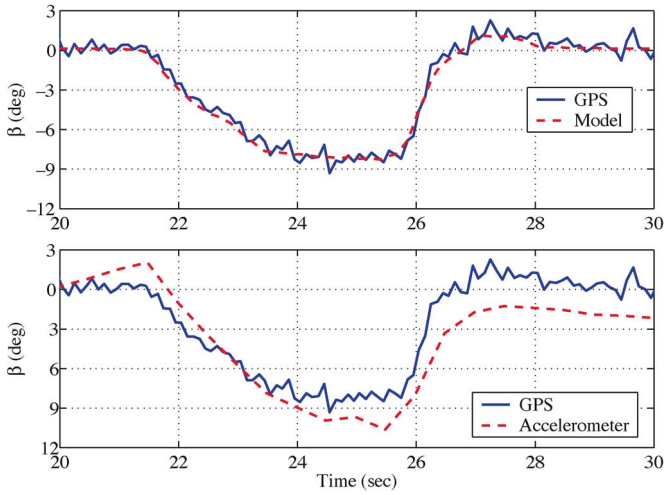

Fig. 5. Comparison of GPS-based and accelerometer-based sideslip estimates.

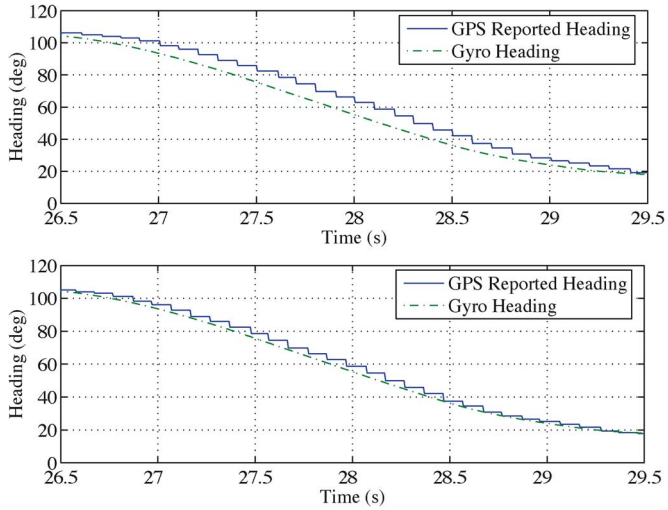

Fig. 6. Effect of GPS measurement latency on sideslip estimate.

can be estimated by integrating a yaw gyroscope during short time intervals. The gyro is initialized, and its bias is estimated during periods of straight driving and then integrated during turning maneuvers to provide the vehicle yaw. Therefore, the vehicle sideslip can be estimated by comparing the GPS course measurements to the integrated yaw gyroscope as shown in the following equation:

$$\hat{\beta}_{\mathrm{GPS}} = \nu_{\mathrm{GPS}} - \int r_{\mathrm{gyro}}. \tag{12}$$

Although using only one GPS antenna to estimate sideslip still requires integration of an inertial sensor (the yaw gyroscope), this method is less sensitive to errors induced from vehicle roll and provides better slip angle estimates that integrate the lateral accelerometer.

A step steer maneuver was performed (at $\sim$7.5 m/s with a yaw rate of $\sim 50^\circ/\mathrm{s}$) in the test vehicle for validation of the proposed algorithms. Fig. 5 shows the raw GPS measured sideslip as well as the sideslip estimate from integrating a lateral accelerometer for this maneuver. The difference in the two measurements arises from calibration errors in the accelerometer, accelerometer signal components due to vehicle roll, as well as drift from integrating the accelerometer.

A major source of error in using the GPS measurement for slip angle estimation arises from the latency of the GPS measurements. The low sample rate of the GPS receiver (10 Hz) introduces a one-half sample period (50 ms) inherent latency. A larger latency component is due to the finite processing and transmission time of the receiver data. Since the slip angle is being measured as the difference between the heading of the vehicle velocity vector as reported by GPS and the heading as reported from the integrated rate gyro, any time offset in the two curves (shown in Fig. 6) results in a slip angle error equal to the time offset multiplied by the rate of turn.

As an example, a 50-ms offset for a $30^\circ/\mathrm{s}$ turn introduces a 1.5° error. Since expected slip angles are on the order of 3°–7°, this represents a large error source and shows the importance of accounting for the GPS latency in order to ensure accurate vehicle state estimates. The time delay latency was accounted for by using time tags in the GPS velocity messages to synchronize the GPS data with the recording system time. Typical values for this delay were within 90–95 ms for the receiver used. The GPS receiver determines velocity by differencing two consecutive carrier wave measurements, which adds an additional latency of one-half the sample rate (50 ms for 10-Hz measurements), resulting in a total offset of 140–145 ms.

VI. One-Antenna GPS/INS Integration

The model given in (1) could be used in estimating the vehicle sideslip in the linear region of the tires. However, uncertainties in the vehicle parameters can lead to bias in the states using a traditional estimator. Therefore, the lateral velocity of the vehicle is estimated by integrating the GPS velocity measurements with the inertial sensors in a kinematic Kalman filter. The term "kinematic" is used because no knowledge of the vehicle model parameters is used. The kinematic Kalman filter uses the accelerometers as inputs and the GPS velocity as a measurement as shown in the following equation:

$$\begin{bmatrix} \dot{u}_y \\ \dot{a}_{\mathrm{bias}} \end{bmatrix} = \begin{bmatrix} 0 & -1 \\ 0 & 0 \end{bmatrix} \begin{bmatrix} u_y \\ a_{\mathrm{bias}} \end{bmatrix} + \begin{bmatrix} 1 \\ 0 \end{bmatrix} (a_y - r u_x)$$
$$u_{y,m}^{\mathrm{GPS}} = C \begin{bmatrix} u_y \\ a_{\mathrm{bias}} \end{bmatrix} \tag{13}$$

where

C	[1 0] if GPS velocity measurements are available;
C	[0 0] if GPS is not available;
u_y	lateral velocity of the vehicle;
a_{bias}	lateral accelerometer bias;
$a_{y,m}$	lateral accelerometer measurement;
$u_{y,m}^{\mathrm{GPS}}$	lateral GPS velocity measurement;
r	vehicle yaw rate;
u_x	vehicle longitudinal velocity.

The lateral GPS velocity measurement can be found by rotating the GPS velocity vector from its east–north coordinates to

lateral and longitudinal velocities in the vehicle frame using the vehicle sideslip estimated with GPS. Thus, we have

$$u_{y,m}^{\mathrm{GPS}} = U_{\mathrm{GPS}} \sin(\hat{\beta}_{\mathrm{GPS}}). \tag{14}$$

A Kalman filter is then applied to the system described by (13). Between GPS measurements and during GPS outages, the Kalman filter simply integrates the accelerometer measurements. When GPS is available, the velocity measurements are used to estimate the accelerometer bias and zero out the sideslip estimate errors that occur from sensor drift. This is known as a loosely coupled GPS/INS integration, since the algorithm uses computed velocity measurements from the GPS receiver.

The Kalman filter comprised a measurement update and time update [30], which is performed at each time step (k). The measurement update is described by

$$\begin{aligned} L_k &= P_k C^T (C P_k C^T + R)^{-1} \\ X_k &= X_k + L_k (y_{\mathrm{meas}} - C X_{k-n}) \\ P_k &= (I - L_k C)_k \end{aligned} \tag{15}$$

where

- L Kalman gain vector;
- P state estimation covariance matrix;
- C observation matrix;
- R sensor noise vector;
- I identity matrix;
- X state estimate vector;
- k current time index;
- n age of the GPS measurement (in samples).

A simple trapezoidal integration time update is described by

$$\begin{aligned} X_{k+1} &= X_k + \frac{\Delta t}{2}(\dot{X}_{k+1} + \dot{X}_k) \\ P_{k+1} &= \Phi P_k \Phi^T + Q_w \end{aligned} \tag{16}$$

where

- $\dot{X}$ calculated from the linear equation in (13);
- Φ discretized Jacobian (**J**) at each time step;
- Q_w discretized process noise matrix.

The trapezoidal (or higher order) integration technique is essential to reduce the amount of error in the vehicle heading estimate. When no current GPS measurements are available, the filter uses the time update step (16) to integrate forward and estimate the vehicle heading from the gyro yaw rate measurement. The Kalman filter provides a current estimate of the vehicle lateral velocity, as opposed to the latent GPS measurement by itself. As noted earlier, it is important that the GPS measurements be compared with heading estimates of the same age in the measurement update. The fact that the lateral accelerometer has no roll compensation must be addressed in properly sizing the process noise matrix for the Kalman filter.

Fig. 7 shows the combination of the GPS velocity measurements with the lateral accelerometer to provide 200-Hz updates of the vehicle sideslip estimation from the step steer test maneuver shown previously. The accelerometer bias estimate for the Kalman filter is also shown. These two plots outline the central idea of this paper: For short time durations, the accelerometer

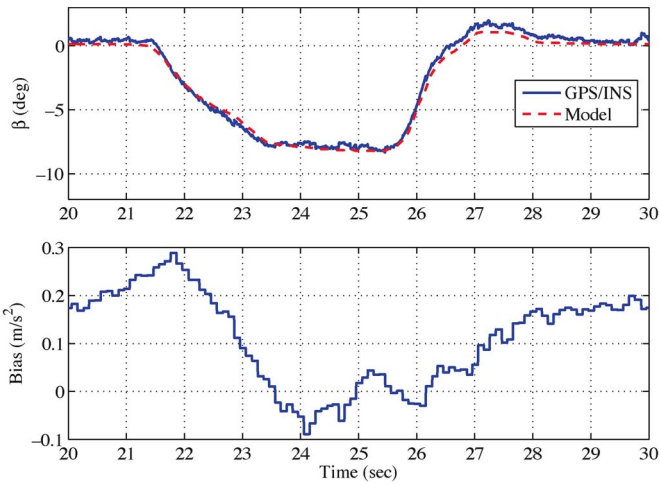

Fig. 7. Combined GPS/INS estimation of sideslip.

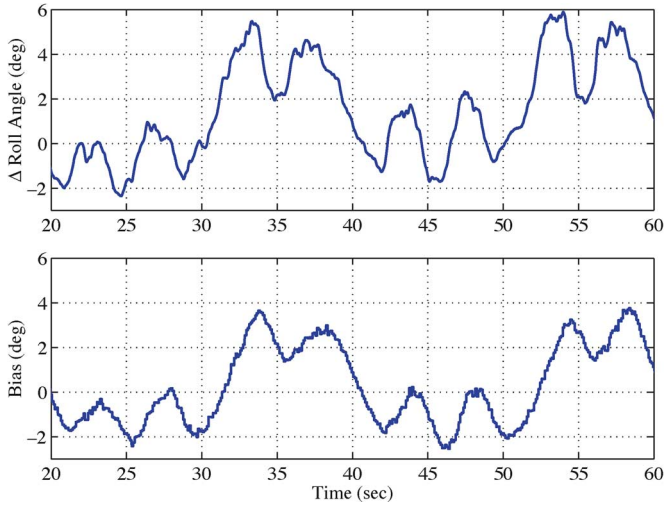

Fig. 8. Measured vehicle roll compared with Kalman filter bias estimation.

measurement could be used to fill in gaps between GPS velocity measurements, but the GPS velocity measurements are required to estimate these sensor errors to provide more accurate estimation than the inertial sensors alone.

The Kalman filter estimation algorithm does track the accelerometer bias that includes vehicle roll as well as any drift in the sensor. Accurate estimation of the accelerometer bias, including offsets due to vehicle roll, allows the Kalman filter to create a better estimate of the vehicle sideslip. Fig. 8 shows an estimate of the change in vehicle roll from integrating a roll gyro and the Kalman filter accelerometer bias estimate. The accelerometer bias estimate is transformed from meters per second squared to degrees of static roll (θ) using the following relationship:

$$\mathrm{bias}_{\mathrm{roll}} = -g \sin(\theta) \tag{17}$$

where g is the gravitational constant. The ability of the Kalman filter to provide a rough estimate vehicle roll can easily be seen in Fig. 8. However, note that the accelerometer bias has a slight

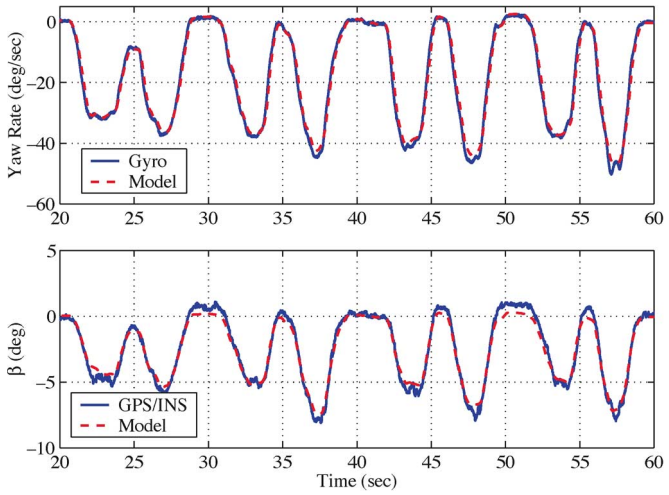

Fig. 9. Measured yaw rate and sideslip angle during cornering maneuvers.

lag from the roll angle. This is due to the inherent lag in the bias estimation from the Kalman filter.

Fig. 9 shows comparisons between the predicted yaw rate and the yaw gyro and between the predicted vehicle sideslip angle and the GPS/INS-measured slip angle. At the speeds of this experimental run, the sideslip angle measurement noise due to the GPS velocity accuracy is approximately 0.4°. Any additional difference between the model and measured sideslip angle can be attributed to vehicle nonlinearities not included in the simple model shown in (1), including nonconstant velocity and a sloping test surface, and lateral velocities due to neglected vehicle roll.

It is interesting to note that the major difference between the model and experimental sideslip occurs along straight-away number 2 (at $t = 30$ s and $t = 50$ s). This is consistent with changing side-slope of the parking garage along that straight-away. Note that the Kalman filter provides a rough estimate of vehicle roll as shown in Fig. 8. However, the magnitude is not exactly the same, and there exists a lag in the roll estimate as mentioned previously. This lag is most evident when the bias is changing due to changing roll angles. The larger the roll velocity, the greater the errors in the roll estimate due to the estimation lag. This motivates the use of a direct measurement of road side-slope and vehicle roll in order to improve the sideslip estimates.

VII. Two-Antenna GPS/INS Integration

In order to improve on the inherent limitation of the one-antenna GPS/INS sideslip estimation, a two-antenna GPS receiver can be used to take into account the effect of road side-slope and vehicle roll on sideslip estimation. The two-antenna system uses integer-resolved carrier phase measurements to prove accurate attitude measurements [31]. When using the two-antenna GPS system, the vehicle yaw is directly measured, which provides a fully observable estimate. By utilizing two antennas, heading estimate errors due to both gyro integration (arising from bias estimate errors, scale factor, integration routine, and integration of a noisy signal) and synchronization of the GPS/INS measurements are eliminated. The two GPS antennas are placed laterally to measure both yaw and roll of vehicle (pitch is neglected since the lateral dynamics are of most interest). The simple roll model, shown previously in Fig. 2, consisting of constant roll center is considered. Yaw and roll measurements from the GPS calibrate the rate gyro bias even when the vehicle is not going straight and enable more accurate heading estimation. With the simple roll center model, greater accuracy is obtained by subtracting out the component of velocity caused by vehicle roll in the GPS velocity measurements.

The GPS measurements, which are unbiased and drift free, can be used to estimate the sensor biases and zero out the state estimate errors. A two-antenna GPS receiver provides yaw angle, roll angle, and velocity vector in the Earth-fixed coordinates

$$\begin{aligned} \psi_m^{\mathrm{GPS}} &= \psi + \text{noise}, & \phi_m^{\mathrm{GPS}} &= \phi_r + \phi_v + \text{noise} \\ U_m^{\mathrm{GPS}} &= U_{\mathrm{antenna}} + \text{noise}, & \nu_m^{\mathrm{GPS}} &= \nu_{\mathrm{antenna}} + \text{noise} \end{aligned} \tag{18}$$

where

ψ_m^{GPS}	yaw angle measurement from GPS;
ϕ_m^{GPS}	roll angle measurement from GPS;
U_m^{GPS}	velocity magnitude measurement from GPS;
U_{antenna}	magnitude of velocity at the GPS antenna;
ν_m^{GPS}	course angle (direction of velocity) measurement from GPS;
ν_{antenna}	direction of velocity at the GPS antenna.

In order to combine the sensor measurements from (4) and (18), the velocity at the vehicle frame must be transposed to the point at the antenna with the velocity addition from vehicle angular velocity. In addition, the transformation from the vehicle-fixed coordinates to the Earth-fixed coordinates has to be applied because the GPS measurements are given in the Earth-fixed coordinates. Assuming the primary GPS antenna is placed on the centerline of the vehicle's roof right above the vehicle CG, the kinematic relationship between GPS measurements and vehicle states is

$$\begin{aligned} u_{Y,\mathrm{antenna}} &= U_{\mathrm{antenna}} \sin(\gamma_{\mathrm{antenna}} - \psi) \\ u_{Y,\mathrm{antenna}} &= (u_{y,\mathrm{frame}} - h_a \dot{\phi}_v \cos\phi_v)\cos\phi \\ &\quad - h_a \dot{\phi}_v \sin\phi_v \sin\phi_r \end{aligned} \tag{19}$$

where

$u_{Y,\mathrm{antenna}}$	lateral velocity at the GPS antenna in the Earth-fixed coordinates;
h_a	vertical distance from roll center to the GPS antenna.

Using the small-angle approximation and assuming the rate of change of vehicle suspension roll is dominant compared with that of road side-slope ($\dot{\phi}_r + \dot{\phi}_v \approx \dot{\phi}_v$), a linear system can be constructed from (4), (18), and (19). The constructed system uses the INS sensors as inputs and the GPS attitude and velocity as measurements. A Kalman filter is then applied to the system to estimate the vehicle states and the sensor biases. Although the two angles ϕ_r and ψ_v are mixed in the original equations, the sum of two angles, i.e., $\phi_t = \phi_r + \phi_v$, can be estimated

correctly. If it is necessary to separate the two angles ϕ_r and ϕ_v, the vehicle dynamics should be considered

$$\begin{bmatrix} \dot{u}_{y,\text{frame}} \\ \dot{a}_{y,\text{bias}} \\ \dot{\psi} \\ \dot{r}_{\text{bias}} \\ \dot{\phi}_t \\ \dot{p}_{\text{bias}} \end{bmatrix} = \begin{bmatrix} 0 & -1 & 0 & u_{x,\text{frame}} & -g & 0 \\ 0 & 0 & 0 & 0 & 0 & 0 \\ 0 & 0 & 0 & -1 & 0 & 0 \\ 0 & 0 & 0 & 0 & 0 & 0 \\ 0 & 0 & 0 & 0 & 0 & -1 \\ 0 & 0 & 0 & 0 & 0 & 0 \end{bmatrix} \begin{bmatrix} u_{y,\text{frame}} \\ a_{y,\text{frame}} \\ \psi \\ r_{\text{bias}} \\ \phi_t \\ p_{\text{bias}} \end{bmatrix} + \begin{bmatrix} 1 & 0 & 0 \\ 0 & 0 & 0 \\ 0 & 1 & 0 \\ 0 & 0 & 0 \\ 0 & 0 & 1 \\ 0 & 0 & 0 \end{bmatrix} \begin{bmatrix} a_{y,m} - r_m \cdot u_{x,\text{frame}} \\ r_m \\ p_m \end{bmatrix} + \text{noise} \quad (20)$$

where

$$\phi_t = \phi_r + \phi_v$$
$$\dot{\phi}_t = \dot{\phi}_r + \dot{\phi}_v \approx \dot{\phi}_v.$$

When GPS attitude measurements are available, we have

$$\begin{bmatrix} \psi_m^{\text{GPS}} \\ \phi_m^{\text{GPS}} \end{bmatrix} = \begin{bmatrix} 0 & 0 & 1 & 0 & 0 & 0 \\ 0 & 0 & 0 & 0 & 1 & 0 \end{bmatrix} \begin{bmatrix} u_{y,\text{frame}} \\ a_{y,\text{frame}} \\ \psi \\ r_{\text{bias}} \\ \phi_t \\ p_{\text{bias}} \end{bmatrix} + \text{noise}. \quad (21)$$

When GPS velocity measurements are available, we have

$$\left[\nu_m^{\text{GPS}}\right] = \begin{bmatrix} \frac{1}{U_{\text{GPS}}} & 0 & 1 & 0 & 0 & \frac{h_a}{U_{\text{GPS}}} \end{bmatrix} \begin{bmatrix} u_{y,\text{frame}} \\ a_{y,\text{frame}} \\ \psi \\ r_{\text{bias}} \\ \phi_t \\ p_{\text{bias}} \end{bmatrix} + \begin{bmatrix} 0 & 0 & -\frac{h_a}{U_{\text{GPS}}} \end{bmatrix} \begin{bmatrix} a_{y,m} - r_m \cdot u_{x,\text{frame}} \\ r_m \\ p_m \end{bmatrix} + \text{noise}. \quad (22)$$

VIII. Experimental Comparison of One- and Two-Antenna GPS/INS Algorithms

The experimental test consisting of eight 80°–90° turns around the top of an uneven parking garage shown previously in Fig. 3 was used to validate the two-antenna sideslip and tire cornering stiffness estimation algorithms. Roll and heading angles from the raw GPS measurements were combined with the INS sensors using the roll center model in Fig. 2. The GPS/INS combination provides higher updates of the vehicle roll and yaw. Comparisons validating the GPS sideslip estimates against truth measurements obtained from a Datron optical velocity sensor as well as covariance analysis of the estimates have been shown [32].

Fig. 10 shows the estimated vehicle sideslip angle sideslips from the one- and two-antenna methods as well as the predicted sideslip angle using the bicycle model (1). The differences between the modeled sideslip angle and the GPS/INS estimated

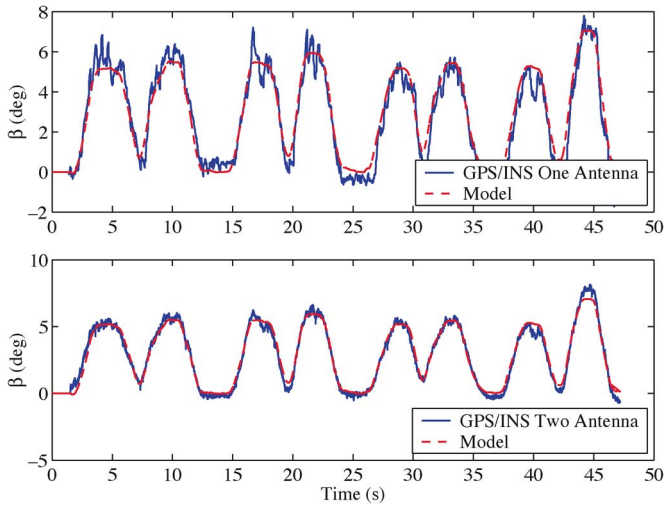

Fig. 10. Comparison of sideslip estimates during cornering maneuvers.

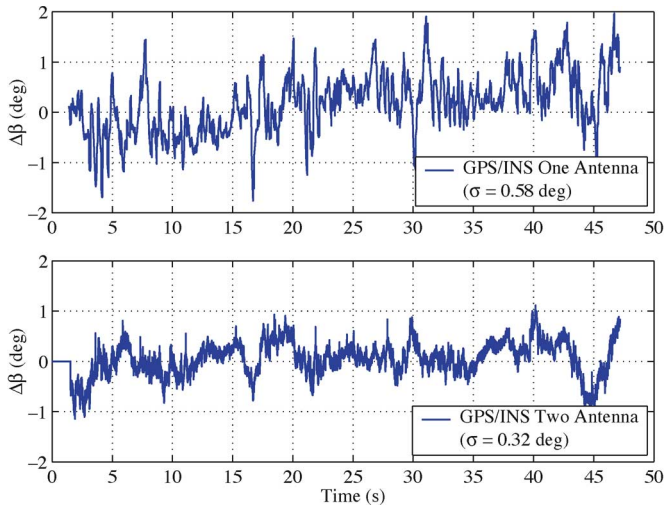

Fig. 11. Difference between the model sideslip and GPS/INS-estimated sideslip.

sideslip angle are shown in Fig. 11. Note that the "errors" are not white, suggesting that there are unmodeled dynamics in the model predicted sideslip. In regions where the errors are white, the sideslip accuracy matches expected values predicted by the covariance analysis in the previous section.

Fig. 12 shows the estimates of the lateral accelerometer bias using the one- and two-antenna methodology as well as the two-antenna measured roll. Although the sideslip estimates from both systems match well with the predicted sideslip produced by the bicycle model, the accelerometer bias estimate using the one-antenna system has large fluctuations, whereas the bias estimate using the two-antenna system remains nearly constant. This is due to the fact that the one-antenna GPS/INS system must estimate changing bias as well as deviations in the lateral accelerometer due to the effects of gravity from road side-slope and vehicle roll. Therefore, the accelerometer bias estimate includes these gravity-based errors as well as any sensor drift. This results in the large changes in the bias estimate shown in Fig. 12 (and previously in Fig. 8). However, because the two-antenna method measures and accounts for the effect of roll, the two-antenna GPS/INS solution can be better optimized

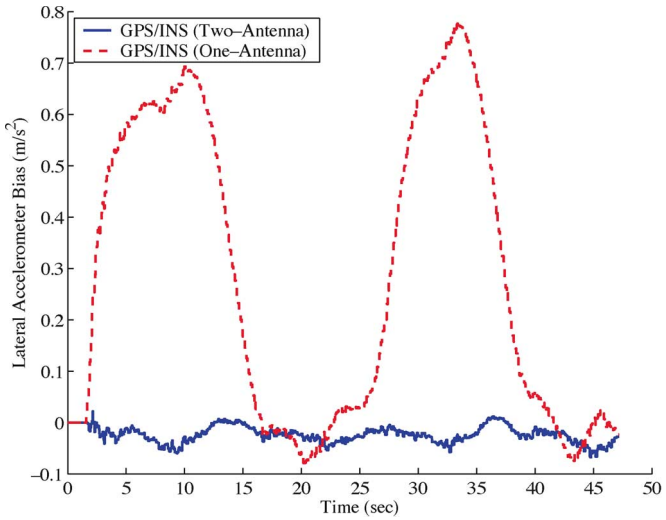

Fig. 12. Comparison of bias estimates and measured vehicle roll.

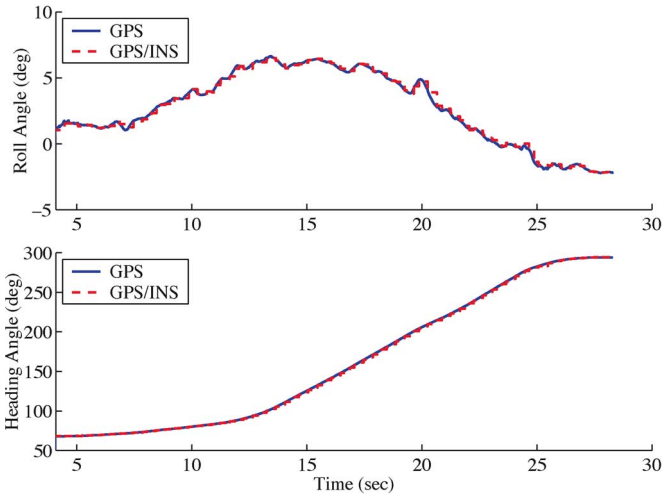

Fig. 13. Vehicle roll and heading angles on a highway ramp.

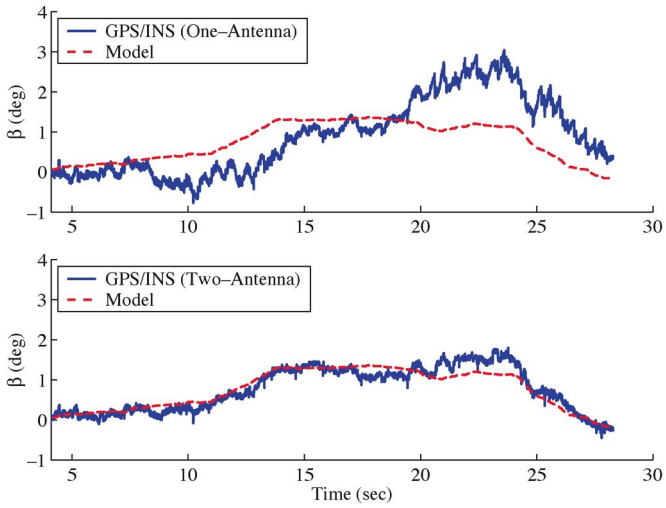

Fig. 14. Comparison of sideslip estimates on a highway ramp.

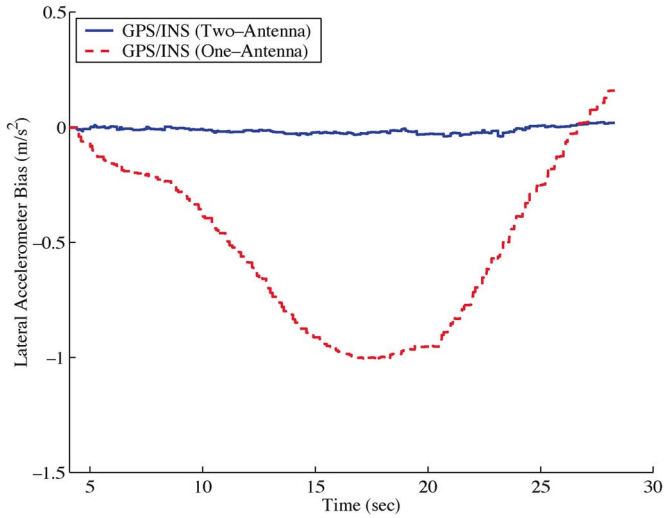

Fig. 15. Comparison of bias estimates on a highway ramp.

such that only slowly varying accelerometer drifts must be estimated. This can be seen by the fact that the accelerometer bias estimate using the two-antenna methodology is fairly constant in Fig. 12. Because the bias estimate using the one-antenna system can track the changes in roll and cancel the effect of gravity roughly, the two systems show similar performance in estimating the vehicle sideslip (shown in Fig. 10), even with a significant level of roll angle as shown at around $t = 6$ s and 31 s in Fig. 12.

The effect of changes in roll on the sideslip estimate is more obvious under more realistic driving conditions. Another experimental test was performed on a highway ramp with considerable side-slope. Fig. 13 displays the roll and heading angles from both the raw GPS measurements and the combination of GPS and INS sensor measurements. Fig. 14 shows the estimated vehicle sideslip angles as well as the model-predicted ones. The road side-slope is taken into account in the model since it affects lateral dynamics of vehicle. The lateral accelerometer bias estimates are also shown in Fig. 15.

As shown in Fig. 13, the roll angle of the vehicle increases during the first 10 s and stays at the maximum for about 5 s. Then, it decreases during the last 10 s. Although these changes in roll can be tracked in the bias estimate term with the one-antenna system, a lag exists estimating the bias (and therefore in estimating the vehicle roll) in the Kalman filter, which degrades the performance of sideslip estimation as discussed previously. The effects of the change in roll angle on the sideslip estimate can be easily seen in Fig. 14. The sideslip angle estimate using the two-dimensional model is underestimated or overestimated when the roll angle increases or decreases, respectively. However, these changes in roll do not corrupt the sideslip estimation with the two-antenna system since the roll is directly measured and compensated.

The tire sideslip angles can also be determined using the methods described above. Figs. 16 and 17 show the predicted and GPS/INS-measured tire sideslip angle of the experimental run on top of the parking garage. Although the one-antenna system has been shown capable of providing good estimates of tire slip angles [33], the two-antenna system gives much better estimates when dealing with small angles as seen in Figs. 16 and 17. This demonstrates the need for accurate roll measurements when determining small tire slip angles.

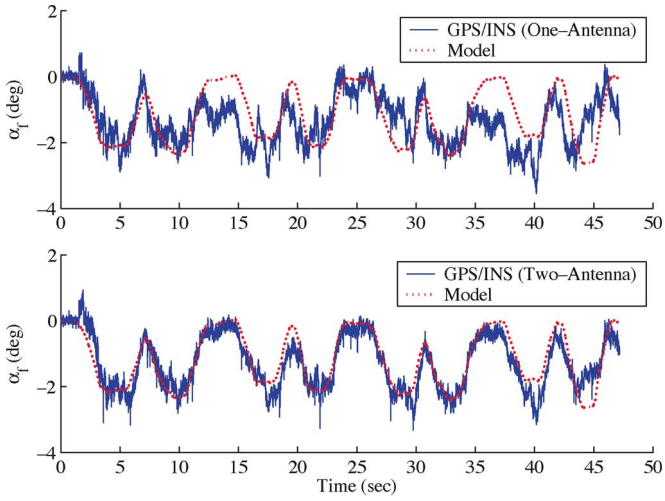

Fig. 16. Measured front tire sideslip angle during cornering maneuvers.

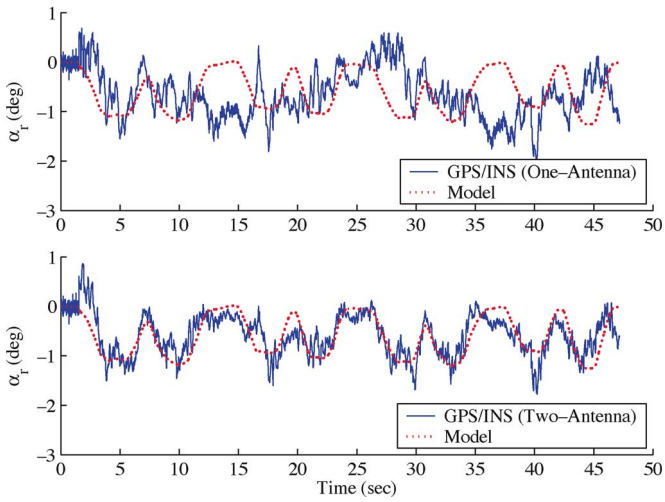

Fig. 17. Measured rear tire sideslip angle during cornering maneuvers.

The tire cornering stiffness was estimated by solving (10) and (11) at each time step using the two-antenna GPS/INS-estimated tire slip angles and lateral accelerometer measurements. The estimates were smoothed using a moving average filter. Fig. 18 shows a plot of the experimentally estimated tire cornering stiffnesses over time during the cornering experiments. It is important to note that the experiments were performed at relatively low velocities (parking lot maneuvers) where the amount of tire sideslip is fairly small (relative to the sensor noises). This results in a less-than-ideal signal-to-noise ratio. However, even at these low speeds, the estimated tire cornering stiffnesses are within 10% of the predicted values. These results would certainly be improved during turning maneuvers at highway speeds (where the signal to noise ratio would be increased). Note that estimates of vehicle sideslip and tire slip using a single GPS antenna have also been shown capable of providing similar estimates of tire cornering stiffness [33].

IX. Conclusion

This paper has shown the feasibility of integrating inertial sensors with GPS measurements to obtain high update sideslip angle of a vehicle. It was first shown that a single GPS antenna/receiver pair could provide improved estimates of vehicle sideslip over existing architectures that rely solely on integrating inertial sensor measurements. The methodology was then extended to combine the GPS measurements with INS measurements to estimate the sideslip and vehicle roll. An estimation method utilizing a two-antenna GPS system to account for road side-slope and vehicle roll was then shown to provide even more accurate (unbiased) high update estimates of the vehicle sideslip and tire sideslip. Additionally, experiments were used to show that the GPS velocity based measurements could be used to estimate the tire cornering stiffnesses on the vehicle.

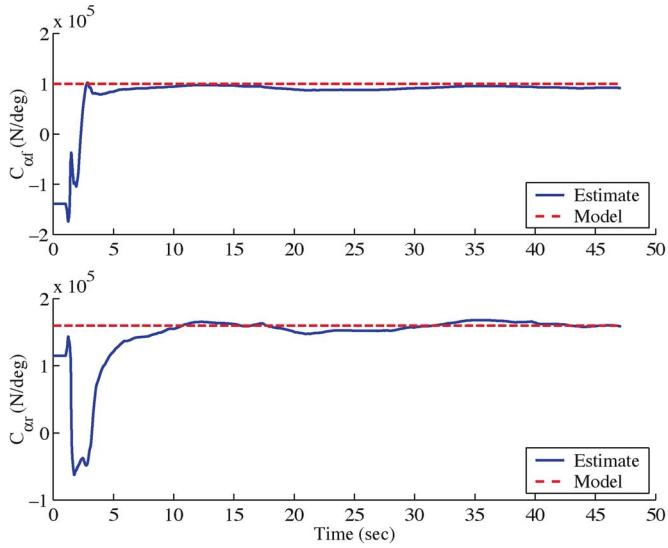

Fig. 18. Estimated tire cornering stiffnesses (per axle).

Acknowledgment

The authors would like to thank Robert Bosch Corporation for providing the test vehicle as well as all of the software and hardware interfaces to collect the experimental data given in this paper.

References

[1] S. Kimbrough, "Coordinated braking and steering control for emergency stops and accelerations," in *Proc. WAM ASME*, Atlanta, GA, 1991, pp. 229–244.
[2] A. T. Van Zanten *et al.*, "Control aspects of the Bosch-VDC," in *Proc. AVEC*, Jun. 1996, pp. 573–607.
[3] ——, "Evolution of electronic control systems for improving the vehicle dynamic behavior," in *Proc. AVEC*, 2002, pp. 7–15.
[4] V. Alberti and E. Babbel, "Improved driving stability by active braking on the individual wheel," in *Proc. Int. Symp. Adv. Veh. Control*, Jun. 1996, pp. 717–732.
[5] A. Hac and M. Simpson, "Estimation of vehicle sideslip angle and yaw rate," presented at the SAE World Congr., Detroit, MI, Mar. 2000, SAE Paper No. 2000-01-0696.
[6] H. E. Tseng, "Dynamic estimation of road bank angle," in *Proc. AVEC*, Ann Arbor, MI, Aug. 2000, pp. 421–428.
[7] U. Kiencke and A. Daiss, "Observation of lateral vehicle dynamics," in *Proc. IFAC*, 1996, pp. 7–10.
[8] J. Farrelly and P. Wellstead, "Estimation of vehicle lateral velocity," in *Proc. IEEE Conf. Control Appl.*, Dearborn, MI, 1996, pp. 552–557.
[9] H. Nishio *et al.*, "Development of vehicle stability control system based on vehicle sideslip angle estimation," presented at the SAE World Congr., Detroit, MI, 2001, SAE Paper No. 2001-01-0137.

[10] V. Morellas, T. Morris, L. Alexander, and M. Donath, "Preview based control of a tractor trailer using DGPS for road departure accidents," in *Proc. IEEE Conf. Intell. Transp. Syst.*, Boston, MA, Nov. 1997, pp. 797–805.
[11] S. Kimbrough, "Coordinated braking and steering control for emergency stops and accelerations," in *Proc. WAM ASME*, Atlanta, GA, 1991, pp. 229–244.
[12] C. E. Cohen, B. W. Parkinson, and B. D. McNally, "Flight tests of attitude determination using GPS compared against an inertial navigation unit," *Navigation: J. Inst. Navig.*, vol. 41, no. 1, p. 83, Spring 1994.
[13] R. Da, G. Dedes, and K. Shubert, "Design and analysis of a high-accuracy airborne GPS/INS system," in *Proc. 9th Int. Tech. Meeting Satellite Division Inst. Navigat. (ION GPS-96)*, Sep. 1996, pp. 955–964.
[14] D. Gebre-Egziabher, R. C. Hayward, and J. D. Powell, "A low-cost GPS/inertial attitude heading reference system (AHRS) for general aviation application," in *Proc. IEEE Position Location and Navigat. Symp.*, Apr. 1998, pp. 518–525.
[15] Z. Berman and J. D. Powell, "The role of dead reckoning and inertial sensors in future general aviation navigation," in *Proc. IEEE Position Location and Navigat. Symp.*, Apr. 1998, pp. 510–517.
[16] A. Masson, D. Burtin, and M. Sebe, "Kinematic DGPS and INS hybridization for precise trajectory determination," in *Proc. 9th Int. Tech. Meeting Satellite Division Inst. Navigat. (ION GPS-96)*, Sep. 1996, pp. 965–973.
[17] D. M. Bevly, A. Rekow, and B. Parkinson, "Evaluation of a blended dead-reckoning and carrier phase differential GPS system for control of an off-road vehicle," in *Proc. ION-GPS Meeting*, Nashville, TN, Sep. 1999, p. 2061.
[18] E. Abbot and D. Powell, "Land-vehicle navigation using GPS," *Proc. IEEE*, vol. 87, no. 1, pp. 145–162, Jan. 1999.
[19] J. Ryu, E. J. Rossetter, and J. C. Gerdes, "Vehicle sideslip and roll parameter estimation using GPS," in *Proc. AVEC*, 2002, pp. 373–380.
[20] J. Farrell, T. Givargis, and M. Barth, "Real-time differential carrier phase GPS-aided INS," *IEEE Trans. Control Syst. Technol.*, vol. 8, no. 4, pp. 709–721, Jul. 2000.
[21] Y. Yang and J. A. Farrell, "Magnetometer and differential carrier phase GPS-aided INS for advanced vehicle control," *IEEE Trans. Robot. Autom.*, vol. 19, no. 2, pp. 269–282, Apr. 2003.
[22] Y. Kubo, T. Kindo, A. Ito, and S. Sugimoto, "DGPS/INS/wheel sensor integration for high accuracy land-vehicle positioning," in *Proc. ION-GPS Meeting*, Nashville, TN, 1999, pp. 555–564.
[23] G. Dissanayake, S. Sukkarieh, E. Nebot, and H. Durrant-Whyte, "The aiding of a low-cost strapdown inertial measurement unit using vehicle model constraints for land vehicle applications," *IEEE Trans. Robot. Autom.*, vol. 17, no. 5, pp. 731–747, Oct. 2001.
[24] H. S. Bae, J. Ryu, and C. Gerdes, "Road grade and vehicle parameter estimation for longitudinal control using GPS," in *Proc. IEEE Conf. Intell. Transp. Syst.*, Oakland, CA, Aug. 2001, pp. 166–171.
[25] R. P. Kornfeld, R. J. Hansman, and J. J. Deyst, "Single antenna GPS based aircraft attitude determination," in *Proc. ION Tech. Meeting*, Long Beach, CA, Jan. 1998, pp. 345–354.
[26] K. Hui, R. Srinivasan, and S. Baillie, "Simultaneous calibration of aircraft position error and airflow angles using differential GPS," *Can. Aeronaut. Space J.*, vol. 42, no. 4, pp. 185–193, Dec. 1996.
[27] D. M. Bevly, J. C. Gerdes, and C. Wilson, "The use of GPS based velocity measurements for measurement of sideslip and wheel slip," *Veh. Syst. Dyn.*, vol. 38, no. 2, pp. 127–147, Aug. 2002.
[28] J. C. Dixon, *Tires, Suspension, and Handling*, 2nd ed. Warrendale, PA: SAE Int., 1996.
[29] P. Yih, R. Jihan, and J. C. Gerdes, "Modification of vehicle handling characteristics via steer-by-wire," in *Proc. Amer. Control Conf.*, Jun. 2003, pp. 2578–2583.
[30] R. Stengel, *Optimal Control and Estimation.* Mineola, NY: Dover, 1994.
[31] R. Hayward, A. Marchick, and J. D. Powell, "Two antenna GPS attitude and integer ambiguity resolution for aircraft applications," in *Proc. ION Tech. Meeting*, San Diego, CA, 1999, pp. 155–164.
[32] D. M. Bevly, R. Daily, and W. Travis, "Estimation of critical tire parameters using GPS based sideslip measurements," in *Proc. SAE Dynamics, Stability, and Controls Conf.*, Novi, MI, Feb. 2006, pp. 87–94.
[33] D. M. Bevly, R. Sheridan, and J. Gerdes, "Integrating INS sensors with GPS velocity measurements for continuous estimation of vehicle sideslip and tire cornering stiffness," in *Proc. ACC*, Arlington, VA, Jun. 2001, pp. 25–30.

David M. Bevly received the B.S. degree from Texas A&M University, College Station, in 1995, the M.S. degree from the Massachusetts Institute of Technology, Cambridge, in 1997, and the Ph.D. degree from Stanford University, Stanford, CA, in 2001, all in mechanical engineering.

He joined the Faculty of the Department of Mechanical Engineering, Auburn University, Auburn, AL, in 2001 as an Assistant Professor. His research interests include control systems, sensor fusion, GPS, state estimation, and parameter identification. His research focuses on vehicle dynamics as well as modeling and control of vehicle systems. Specifically, he has developed algorithms for the control of off-road vehicles and methods for identifying critical vehicle parameters using GPS and inertial sensors.

Jihan Ryu received the B.S degree in naval architecture and ocean engineering from Seoul National University, Seoul, Korea, and the M.S. and Ph.D. degrees in mechanical engineering from Stanford University, Stanford, CA, in 2000 and 2004, respectively.

He is currently a Senior Researcher with General Motors R&D, Warren, MI. His research interests include modeling, identification, and control of dynamic systems.

J. Christian Gerdes received the Ph.D. degree in mechanical engineering from the University of California, Berkeley, in 1996.

He is an Associate Professor with the Design Group, Department of Mechanical Engineering, Stanford University, Stanford, CA. He is also the Director of the Dynamic Design Laboratory (DDL), which focuses on the integration of dynamic modeling and control into the mechanical design process. Current activities in the DDL include ground vehicle state estimation, drive-by-wire control, driver assistance systems, and control of homogeneous charge compression ignition engines.

Dr. Gerdes received the Presidential Early Career Award for Scientists and Engineers in 2002.